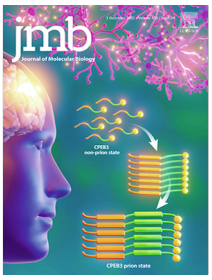

Molecular Characterization of an Intrinsically Disordered Chaperone Reveals Net-Charge Regulation in Chaperone Action

Chang Ren [1,†], Yongxin Zheng [1,†], Chunlan Liu [1], Jun Mencius [1], Zhili Wu [1] and Shu Quan [1,2,*]

*1 - **State Key Laboratory of Bioreactor Engineering,** East China University of Science and Technology, Shanghai Collaborative Innovation Center for Biomanufacturing (SCICB), Shanghai 200237, China*
*2 - **Shanghai Frontiers Science Center of Optogenetic Techniques for Cell Metabolism,** Shanghai 200237, China*

Correspondence to Shu Quan: State Key Laboratory of Bioreactor Engineering, East China University of Science and Technology, 130 Meilong Rd, Shanghai 200237, China. *shuquan@ecust.edu.cn (S. Quan)*
https://doi.org/10.1016/j.jmb.2021.167405
Edited by J. Buchner

Abstract

Molecular chaperones are diverse biomacromolecules involved in the maintenance of cellular protein homeostasis (proteostasis). Here we demonstrate that in contrast to most chaperones with defined three-dimensional structures, the acid-inducible protein Asr in *Escherichia coli* is intrinsically disordered and exhibits varied aggregation-preventing or aggregation-promoting activities, acting as a "conditionally active chaperone". Bioinformatics and experimental analyses of Asr showed that it is devoid of hydrophobic patches but rich in positive charges and local polyproline II backbone structures. Asr contributes to the integrity of the bacterial outer membrane under mildly acidic conditions *in vivo* and possesses chaperone activities toward model clients *in vitro*. Notably, its chaperone activity is dependent on the net charges of clients: on the one hand, it inhibits the aggregation of clients with similar net charges; on the other hand, it stimulates the aggregation of clients with opposite net charges. Mutational analysis confirmed that positively charged residues in Asr are essential for the varied effects on protein aggregation, suggesting that electrostatic interactions are the major driving forces underlying Asr's proteostasis-related activity. These findings present a unique example of an intrinsically disordered molecular chaperone with distinctive dual functions—as an aggregase or as a chaperone—depending on the net charges of clients.

Introduction

Environmental changes directly threaten cell viability, and cell adaptability to environmental stresses depends on an elaborate proteostasis network in which molecular chaperones orchestrate various processes to maintain a functional proteome. In response to protein-unfolding stresses, such as oxidative, acidic, and thermal stresses, which can severely damage cells in seconds or minutes,[1–3] a set of molecular chaperones are induced or activated, including Hsp26, Get3, Hsp33, and HdeA.[4–7] These chaperones have evolved specialized mechanisms for rapidly sensing environment changes and protecting cellular proteins from unfolding stress.[8–10] Once induced or activated, these chaperones can bind unfolded clients and prevent their aggregation. When stress subsides, the activated chaperones return to their original inactive state and release the clients, which are then refolded by canonical chaperones.

Whereas canonical chaperones (e.g., Hsp60, Hsp70, Hsp90, and Hsp100) utilize cycles of ATP binding and hydrolysis-induced conformational changes to bind client proteins,[11] the functions of

some ATP-independent chaperones are strongly dependent on intrinsic structural disorder. The disordered regions in these chaperones enable them to bind and protect multiple clients and regulate chaperone activity.[12,13] For instance, the partial unfolding of the redox-regulated chaperone Hsp33 in response to oxidative stress results in the formation of a disordered linker region, which can capture protein-folding intermediates.[14] Similar to Hsp33, the acid-activated chaperone HdeA has no discernible chaperone activity under normal conditions. At pH 2, the rapid transformation of HdeA from a well-folded and inactive dimer into a partially disordered and active monomer exposes the disordered and hydrophobic client-binding surface of HdeA.[7,15]

The main driving forces of chaperone action are hydrophobic and electrostatic interactions.[16] Chaperones recognize the exposed hydrophobic patches of their clients.[17,18] However, it is increasingly recognized that initial chaperone-client interactions are largely facilitated by electrostatic forces.[19,20] Compared with hydrophobic interactions, electrostatic interactions are the long-range forces that drive the rapid association between chaperones and clients.[21] Many chaperones require electrostatic interactions for effective client-binding, such as GroEL, Hsp90, Hsp70, and Spy.[16,19,22–24] Moreover, highly charged molecules, including nucleic acids,[25,26] polyphosphates,[27] and the recently reported heat-resistant obscure (Hero) proteins,[28] can efficiently provide protection against protein aggregation. Although the mechanisms by which these molecules implement chaperone activities have not been well understood, electrostatic forces may be important to the chaperone activities of these highly charged molecules.

The periplasm of *Escherichia coli* is particularly vulnerable to environmental stresses because molecules below ~600 Da can freely diffuse through the outer membrane.[29] To cope with periplasmic unfolding stresses, *E. coli* has evolved a series of stress-activated or stress-induced chaperones. For example, Spy is strongly induced by butanol or tannic acid and HdeA is activated by extreme acidic stress.[7,30] The *asr* gene was identified to have high induction levels under moderate external acidic condition (pH 4.0–5.0).[31] Although this phenomenon was reported two decades ago, whether Asr is involved in protein quality control and the mechanisms underlying its functions in *E. coli* remain highly enigmatic.

Here, we demonstrate that the poorly characterized *E. coli* gene *asr* encodes a stress-induced intrinsically disordered protein (IDP) that carries highly positive charges and contributes to the integrity of the outer membrane under moderate acidic stress conditions. Using *in vitro* chaperone assays, we demonstrated that Asr alternates its function as a chaperone that protects against protein aggregation and as an aggregase that promotes protein aggregation. This transition is regulated by the net charges of its client: when the client carries similar net charges with Asr, Asr inhibits its aggregation; when the client carries the opposite net charges to Asr, Asr promotes its aggregation. We further show that the positively charged residues of Asr are necessary for its anti-aggregation or aggregation-promoting activities. Our findings reveal the physiological function of Asr in regulating protein homeostasis in the cell envelope, disclose a possible working model of highly charged ATP-independent chaperones, and provide a reference for the artificial design of similar chaperones with potential biotechnological and therapeutic applications.

Results

Asr is a highly charged, hydrophilic, and intrinsically disordered protein

Asr has a signal sequence that targets it to the Sec-translocon, resulting in its translocation into the periplasm of *E. coli*.[32] The only hydrophobic amino acids in the mature sequence of Asr are alanine and proline (~28% and 10% of the total residues, respectively), which prevent structural core packing[33,34] (Table S1). The protein lacks hydrophobic patches (Figure 1(a)) according to the Kyte-Doolittle hydrophobicity scale.[35] In addition, Asr is almost exclusively composed of hydrophilic amino acids and is enriched in basic amino acids (~21% lysine and 10% histidine,Table S1, Figure 1(a)). Given the lack of obvious hydrophobic motifs that drive the protein folding of Asr, we considered the possibility that Asr lacks well-defined secondary structures. Indeed, disorder propensity analysis of Asr with the IUPred server[36] predicted an entirely disordered structure (Figure 1(a)). We then purified Asr and analyzed its secondary structures through circular dichroism (CD) spectroscopy: The CD spectrum of Asr had a minimum ellipticity at 198 nm and a value close to zero at 220 nm, supporting the predicted overall disordered structure (Figure 1(b)). Moreover, the random-coil conformation of Asr remained unchanged even under denaturing conditions (e.g., extremely acidic pH and high concentrations of urea,Figure 1(b) and (c)).

Intrinsically disordered proteins (IDPs) are devoid of consolidated secondary and tertiary structures at a full protein length scale, but some local structures may exist at the amino acid and short peptide levels.[37–39] The disordered regions in IDPs may form well-defined polyproline II (PPII) backbone structures that can be adopted (with varying propensities) by apparently any type of amino acid.[40–42] These PPII structures serve as recognition motifs in some protein–protein interactions.[43] The CD spectrum of Asr shows two characteristic PPII peaks, a positive peak centered at approxi-

mately 218 nm and a minimum peak at 198 nm[44] (Figure 1(b)). To confirm the presence of PPII structures, we investigated whether these characteristic peaks could be stabilized by low temperatures.[44–46] By comparing the CD spectra of Asr at 5 °C and 85 °C, we found that the magnitude of the two peaks increased with decreasing temperature (Figure 1(d)). We subsequently measured temperature-induced structural changes in Asr through CD spectroscopy and detected a significant correlation between ellipticity at 198 nm and temperature (Figure 1(e)). This correlation indicated the destabilization of the PPII structure at increasing temperatures.[44,45]

Finally, we investigated whether Asr, with a large number of basic residues, possesses any membrane-binding activity. Sulfate dodecyl sodium (SDS) micelles are widely used as model membranes for studying the binding of IDPs to lipid membranes, and SDS has been reported to induce conformational changes in IDPs.[47,48] In the presence of SDS, the CD spectrum of Asr

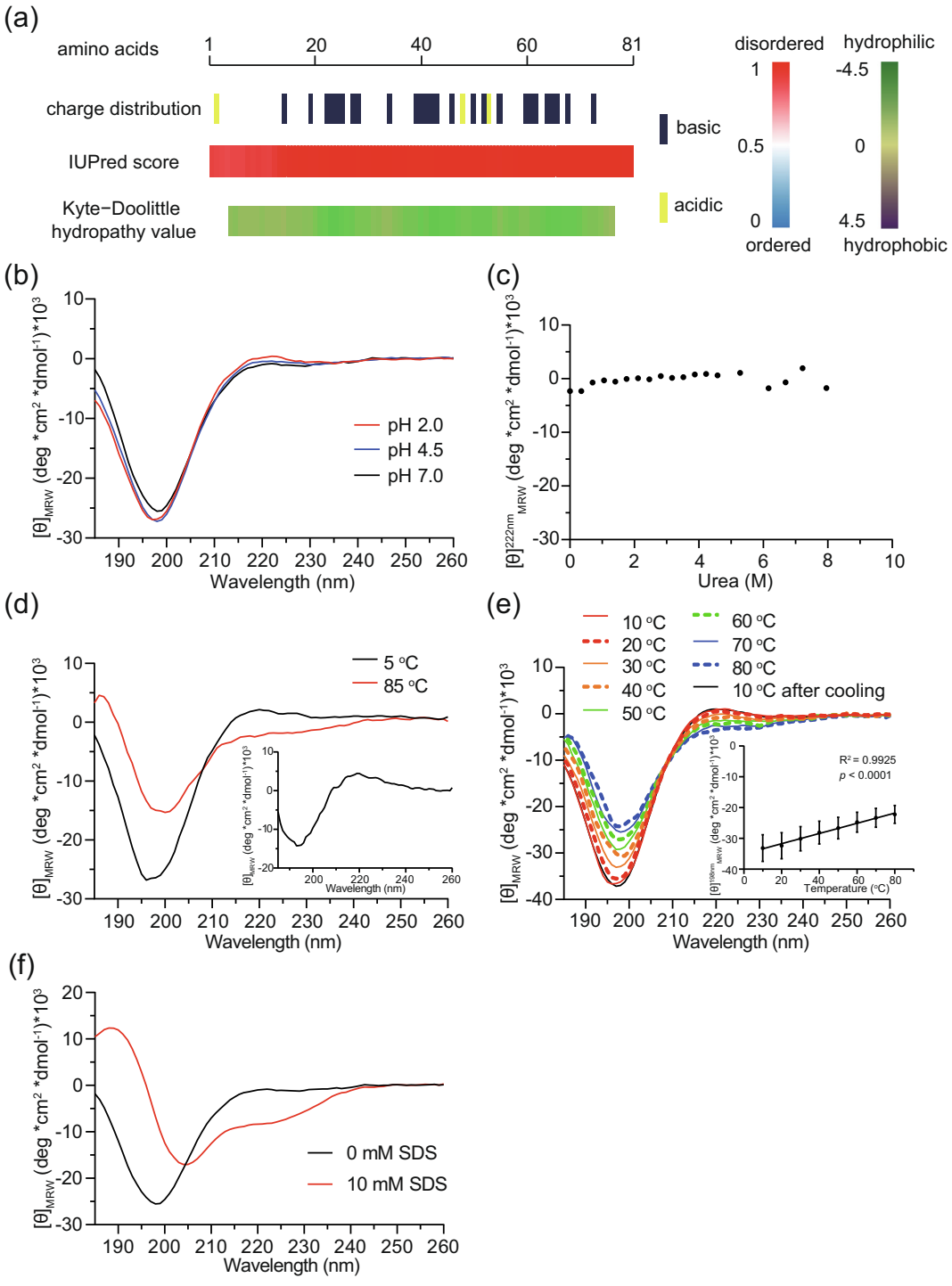

resembled the CD spectra of α-helical proteins (Figure 1(f)), implying that Asr may interact with lipid membranes. We then incubated Asr with liposomes made from *E. coli* membrane lipids and examined the distribution of Asr after centrifugation. Although Asr itself is highly soluble in water, the presence of Asr in pellets containing liposomes suggested that Asr has membrane-binding capacity (Figure S1). These observations demonstrated that the highly positively charged and hydrophilic protein Asr is intrinsically disordered but contains some local structures, including PPII structures, and can thus bind lipid membranes.

Stress-induced accumulation of Asr contributes to the maintenance of outer membrane integrity

We compared the mRNA abundance of the *asr* gene upon incubation of *E. coli* at neutral pH (pH 7.0) and under a mildly acidic condition (pH 4.5). We found that the mRNA abundance of the *asr* gene increased nearly 1000 times under the mildly acidic condition. This result was consistent with a previous microarray study[49] (Figure 2(a)). In addition, after examining the *E. coli* community gene expression database—which provides an extensive collection of gene expression data from over 1200 experiments (GenExpDB, http://genexpdb.ou.edu/index.php)—we found that stress conditions apart from external acidification may strongly induce the expression of the *asr* gene (e.g., heavy metal ion exposure, alcohol exposure, and oxidative conditions; Figure 2(b)). Most of these conditions are known to cause protein aggregation and induce the transcription of genes encoding known chaperones, such as Spy, HdeA/B, and GroEL/S.

Given that the transcription of the *asr* gene is highly up-regulated under various protein unfolding stress conditions, we investigated whether the Asr protein can act as a chaperone. Chaperone-deficient cells often exhibit pleiotropic phenotypes under normal or stress conditions.[27,50] We observed that deletion of the *asr* gene impaired cell growth under the mildly acidic condition (Figure 2(c)). We also observed that the cell growth of the *asr* deletion strain partially restored (up to 50–70% of the wild-type strain level) after complementation of Asr with a low-copy-number plasmid, which expresses *asr* under the control of its own acid-inducible promoter (Figure 2(c)).

Because Asr can bind liposomes (Figure S1), we determined whether Asr contributes to the maintenance of membrane integrity. Cells with membrane defects have increased sensitivity to SDS/EDTA and novobiocin.[51] Therefore, we tested the sensitivity of wild-type *E. coli* and *asr* deletion strains to SDS/EDTA and novobiocin. We cultivated both strains to the stationary phase in low-phosphate-glucose-salt media (LPM)[32] buffered at different pH values and then exposed them to SDS/EDTA and novobiocin at pH 7.0 in lysogeny broth (LB) plates (Figure 2(d)). When cultured at neutral pH, no growth differences were observed in either strain on plates containing SDS/EDTA or novobiocin. By contrast, when previously cultured under the mildly acidic condition, the *asr* deletion strain showed significant growth defects on SDS/EDTA or novobiocin-containing plates compared with wild-type *E. coli*, indicating that the *asr* deletion strain developed more severe membrane damage under mildly acidic stress (Figure 2(d)).

The two outer membrane nonspecific porins OmpA and OmpC are involved in the maintenance of membrane integrity, and their absence induces sensitivity to SDS/EDTA.[52,53] Therefore, we determined whether Asr induced by acid stress plays a role in regulating the steady-state levels of these porins. To this end, we compared the levels of OmpA and OmpC in wild-type *E. coli* with those of the *asr* deletion strain under mildly acidic conditions. The two strains had similar OmpA levels (Figure S2), but the wild-type *E. coli* accumulated significantly more OmpC than the *asr* deletion strain (Figure 2(e)). This difference was not due to transcriptional changes in the *ompC* gene in the *asr* deletion strain (Figure S3). Thus, these results suggested that Asr contributes to the maintenance of

Figure 1. Computational prediction and biophysical characterization of Asr. (a) *In silico* analyses of the charge distribution, disordered content, and hydrophobicity of Asr. Predictions were performed with the amino acid sequences of Asr without its N-terminal signal peptide. Basic amino acids (arginine, lysine, and histidine) are colored in dark blue, and acidic amino acids (aspartate and glutamate) are colored in yellow. The analysis of disordered content and hydrophobicity is based on the IUPred server (https://iupred2a.elte.hu/) and the Kyte-Doolittle scale (https://web.expasy.org/protscale/), respectively. (b) CD spectra of Asr at the indicated pH values. (c) CD signals of urea-denatured Asr at a wavelength of 222 nm, plotted against urea concentration. (d) CD spectra of Asr at 5 °C and 85 °C. Inset: changes in CD signals were calculated by subtracting CD signals at 85 °C from those at 5 °C. (e) CD spectra of Asr at different temperatures (from 10 °C to 80 °C). Inset: CD signals at a wavelength of 198 nm, plotted against temperature. Student's *t* test was used in determining the *p* value. (f) CD spectra of Asr in the presence or absence of 10 mM SDS. Experiments were conducted at least three times, and representative spectra are shown. Data were presented as the mean ± SD.

the integrity of the outer membrane and directly or indirectly affects OmpC proteostasis under mildly acidic conditions.

Asr can suppress or promote protein aggregation

Molecular chaperones recognize unfolded proteins and prevent them from irreversible aggregation.[17] To determine whether Asr serves as a generic molecular chaperone, we assessed the chaperone activity of Asr by analyzing its influence on the aggregation of a variety of model chaperone client proteins. We first tested the effect of Asr on the heat-induced aggregation of malate dehydrogenase (MDH) and found that Asr inhibited MDH aggregation in a dose-dependent manner

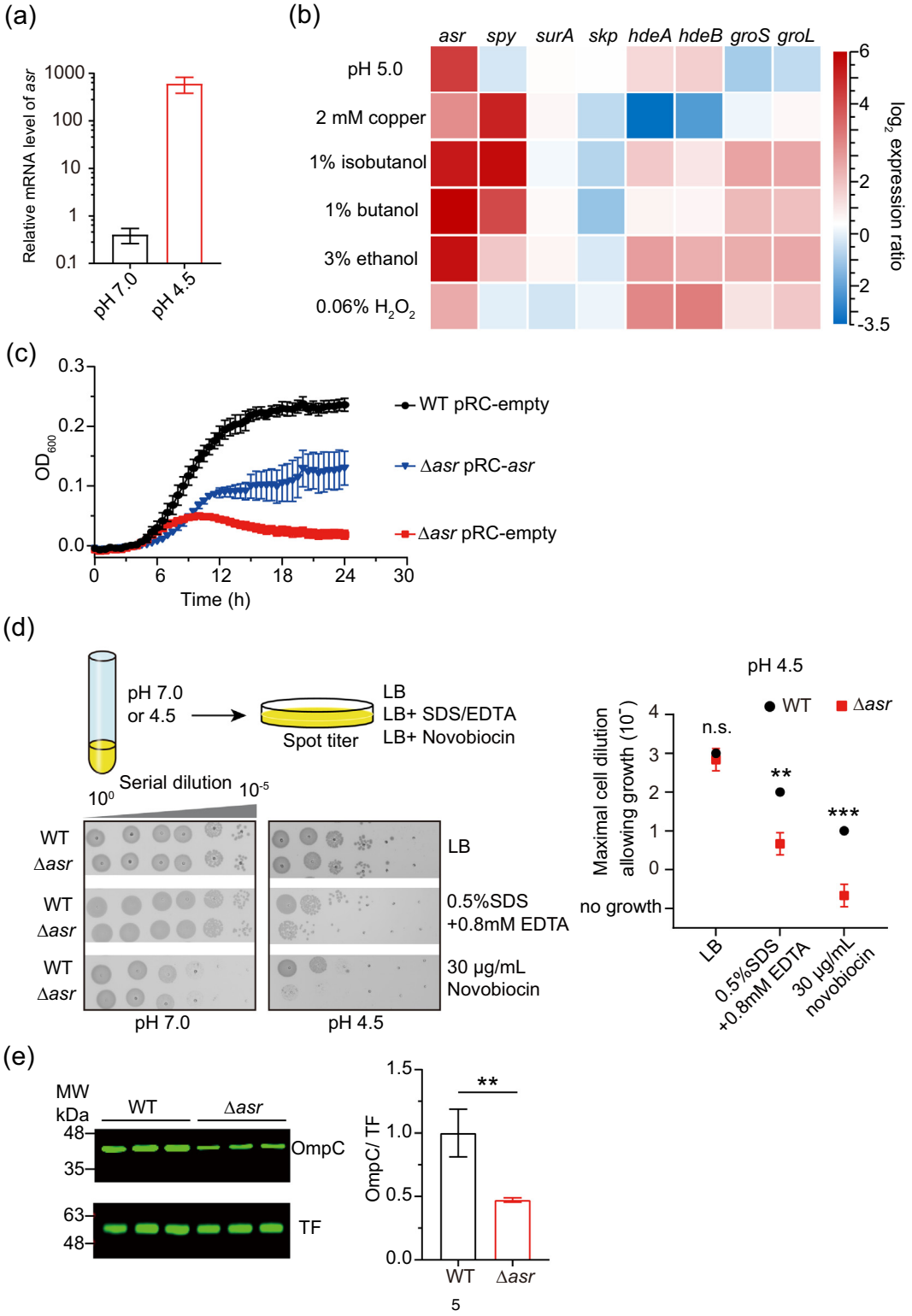

(Figure 3(a)). Analysis of the effects of Asr on chemically denatured MDH revealed similar results (Figure S4(a)). Given that Asr is strongly induced by mildly acidic stress, especially at pH 4.5 (Figure 2(a)), we determined whether Asr exerts protein-protective effects under mildly acidic conditions. We first analyzed the influence of Asr on the aggregation of MDH at pH 4.5. The presence of Asr significantly inhibited the aggregation of MDH subjected to thermal stress at pH 4.5 (Figure S4(b)). Importantly, we found that the anti-aggregation activity of Asr at pH 4.5 was not restricted to MDH and observed similar outcomes for two other classic chaperone clients, luciferase (Luc) and citrate synthase (CS) (Figure 3(c) and (e)).

However, when we tested the potential influence of Asr on the heat-induced aggregation of Luc at pH 7.5—a common pH value for Luc aggregation assays[25–27]—we unexpectedly found that Asr promoted the heat-induced aggregation of Luc in a dose-dependent manner (Figure 3(d)). Notably, this phenomenon cannot be explained by structural changes in Asr or Luc at different pH values as the CD spectra revealed no major differences between their secondary structures at pH 4.5 and those at pH 7.5 (Figures 1(b) and S5). It thus appears that Asr exerts anti-aggregation effects on client proteins at acidic pH, while it exerts pro-aggregation effects on some client proteins at neutral pH.

The chaperone-like activity of Asr depends on the net charges of client proteins

Considering the possible causes of the apparently opposite activities of Asr, we speculated that the activities are related to differences in the overall net charges of client proteins at different pH values. For example, at pH 4.5, which is lower than the isoelectric point (pI) of Asr and all the tested chaperone clients (Table 1), the proteins both carried positive net charges, and Asr exerted anti-aggregation activity under this condition (Figures 3(c), (e), and S4(b)). By contrast, at pH 7.5, at which Asr and Luc carried opposite net charges (Table 1), Asr exerted a pro-aggregation effect on Luc (Figure 3(d)). The findings for MDH are informative: at pH 7.5, MDH and Asr carried positive net charges, and Asr exerted anti-aggregation effects on MDH at this pH. Finally, thermal aggregation assays conducted at pH values at which MDH, Luc, and CS carried negative net charges and Asr had positive net charges (Table 1) revealed the pro-aggregation effects of Asr (Figures 3(b), (d), (f), and S6). These results demonstrated that Asr could inhibit the aggregation of similarly charged clients and promote the aggregation of oppositely charged clients, indicating that net charge is a determinant of the context-specific chaperone activities of Asr.

To rule out the possibility that the observed effect of Asr on protein aggregation is simply due to nonspecific charge-charge interactions, we searched for proteins localized in the periplasm of *E. coli* with the following properties: i) highly charged, ii) hydrophilic, and iii) intrinsically disordered (Figure S7). We then tested their potential influences on the aggregation of MDH and Luc. None of the three examined proteins exerted similar aggregation-related effects resembling Asr. This result showed that the Asr sequence, rather than nonspecific interactions among charged proteins, somehow mediates the proteostasis-related activities of Asr. Collectively, these results revealed a distinctive mechanism by which Asr promotes or suppresses protein aggregation according to the net charges of client proteins.

Figure 2. Asr is a stress-inducible protein that contributes to the maintenance of membrane integrity under mildly acidic conditions. (a) Quantitative real-time PCR analysis of the mRNA abundance of the *asr* gene prepared from wild-type *E. coli* (WT) and the *asr* deletion mutant strain (Δ*asr*), grown in LPM buffered at different pH values to mid-log phase. The mRNA levels of the *asr* gene were normalized to the transcriptional levels of the housekeeping gene *dnaQ*. (b) Heat map of changes in the transcriptional levels of the indicated genes after stimulation of *E. coli* with the indicated stresses. Data were downloaded from the *E. coli* expression database GenExpDB. (c) Growth kinetics of the indicated strains grown in LPM buffered at pH 4.5. The pRC plasmid with a low copy number was generated based on pBAD43 by replacing the L-arabinose operon with the genomic operon of the *asr* gene. A pH of 4.5 can trigger the expression of *asr* from the pRC-asr vector. Cells harboring the empty vector pRC-empty were used as a control. (d) Analysis of SDS/EDTA and novobiocin sensitivity of WT and Δ*asr*. Stationary phase cultures grown in LPM buffered at the indicated pH values were 10-fold serially diluted, spotted onto LB plates supplemented with 0.5% SDS/0.8 mM EDTA and 30 μg/mL novobiocin and LB plates without supplementation. All plates were incubated at 37 °C overnight. Maximal cell dilutions that allowed the growth of WT and Δ*asr* under the indicated conditions were quantified and compared. Experiments were conducted for at least three times, and representative plates are shown. (e) The amount of OmpC in WT and Δ*asr* grown in LPM buffered at pH 4.5 was monitored through immunoblotting with an anti-OmpC primary antibody. The amount of OmpC was quantified and is presented as a bar chart. Endogenous trigger factor (TF) protein was used as a loading control. Student's *t* test was used to determine the *p* value (n.s., nonsignificant, $^{**}p < 0.01$, $^{***}p < 0.001$). Data were presented as the mean ± SD.

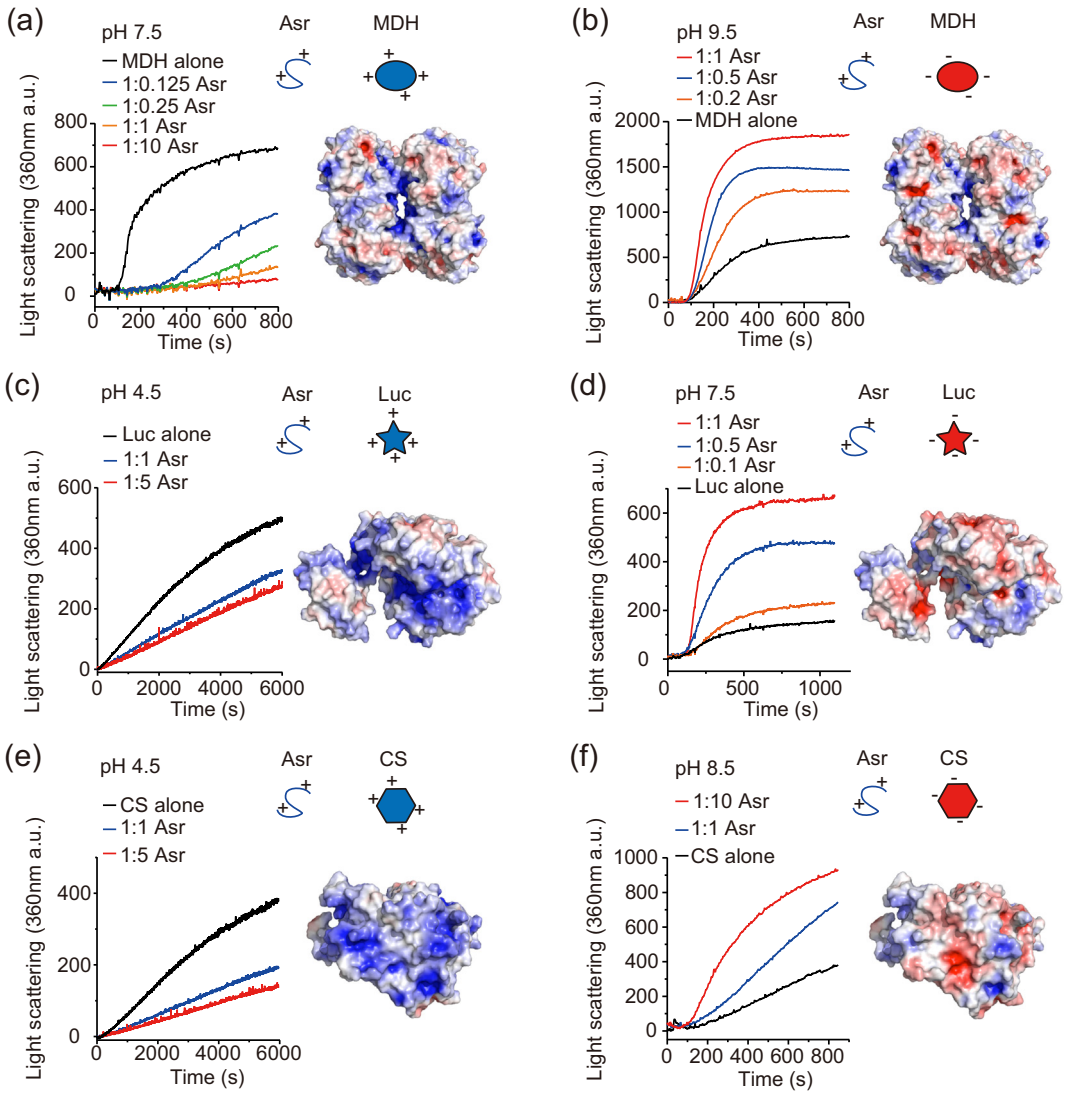

Figure 3. pH regulation of the conditional chaperone activity of Asr in preventing protein aggregation. (a and b) Aggregation of thermally denatured MDH alone, or in the presence of increasing amounts of Asr (ratios given are client: Asr) at pH 7.5 (a) and pH 9.5 (b). The distribution of positive (blue) and negative (red) surface charges on MDH (PDB: 1MLD) at pH 7.5 (a) and pH 9.5 (b) is shown. (c and d) Aggregation of thermally denatured Luc alone, or in the presence of increasing amounts of Asr at pH 4.5 (c) and pH 7.5 (d). The distribution of positive and negative surface charges on Luc (PDB: 1LCI) at pH 4.5 (c) and pH 7.5 (d) is shown. (e and f) Aggregation of thermally denatured CS alone, or in the presence of increasing amounts of Asr at pH 4.5 (e) and pH 8.5 (f). The distribution of positive and negative surface charges on CS (PDB: 3ENJ) at pH 4.5 (e) and pH 8.5 (f) is shown. When the pH value is lower than the isoelectric point of the client, positive charges outweigh negative charges on the surface of the client. When the pH value is higher than the isoelectric point of the client, negative charges are dominant on the surface of the client. Protein aggregation was monitored based on light scattering at 360 nm. The electrostatic surface potential was calculated in PyMOL, and the Adaptive Poisson-Boltzmann Solver tools 2.1 plugin (http://www.poissonboltzmann.org) was used. A color scale for charge distribution from −5 to 5 was used. Experiments were conducted at least three times, and representative curves are shown.

Extreme positive charges of Asr are essential for its effects on protein aggregation

Our results raised several intriguing conceptual questions, particularly with regard to the mechanism by which Asr affects protein aggregation and the potential role of the Asr sequence in this process. When the amino acid composition of Asr was compared with that of the *E. coli* proteome, Asr showed enrichment of basic amino acid residues, and thus it has the highest pI

Table 1 Electrostatic parameters of different proteins

Protein	Isoelectric point (pI)	Overall net-charge property of the protein[a]			
		pH 4.5	pH 7.5	pH 8.5	pH 9.5
MDH	8.5	+	+	n.a.	-
Luc	6.4	+	-	-	-
CS	7.0	+	-	-	-
Asr	10.4	+	+	+	+

[a] The net-charge property of the protein: +, positive; −, negative.

value among the periplasmic proteins in *E. coli* (Figures S7(c) and S8). We explored the influence of the positively charged residues of Asr on protein aggregation.

We first constructed a variant of Asr by replacing lysine with glutamic acid to obtain a negatively charged protein (Asr_{neg}, pI = 4.68; Figure 4(a) and (b)). The biophysical characteristics of Asr_{neg} are similar to those of wild-type Asr, both having an overall random coil conformation (Figure S9(a)), high hydrophilicity, and high proportions of charged residues (although with opposite charges). Thus, we expected that Asr_{neg} would have opposite effects on protein aggregation compared with wild-type Asr. However, upon testing the influence of Asr_{neg} on the heat-induced aggregation of MDH, we found that Asr_{neg} did not affect MDH aggregation (notably, tests were performed with the differentially charged MDH at different pH values; Figure 4(c)–(f)). These results implied that the positive charges of Asr are essential for its effects on protein aggregation.

Upon examining the Asr sequence, we observed that its lysine residues were often directly adjacent to histidine residues (Figure 4(a)). To assess the functional effects of positively charged Asr residues, we synthesized a peptide (KKHH repeats, pI = 10.9) with lysine and histidine repeats connected by glycine and serine linkers (GGSGGS). We set the total length (80 amino acids) of the KKHH repeat sequence close to that of wild-type Asr (81 amino acids; Figure 4(g)) so that this synthesized peptide had biophysical characteristics similar to those of wild-type Asr in charge, hydrophilicity, and structurally intrinsic disorder (Figure S9(b)).

We then tested the influence of the KKHH repeat sequence on the heat-induced aggregation of MDH. Similar to Asr, the KKHH repeat sequence suppressed the aggregation of positively charged MDH at pH 7.5 but promoted the aggregation of negatively charged MDH at pH 9.5 (Figure 4(h) and (j)). Strikingly, the KKHH repeat sequence, derived from the extremely positively charged Asr, was more efficient in preventing and promoting aggregation than Asr (Figure 4(i) and (k)). These results showed that the positively charged residues within Asr, rather than its specific amino acid sequence *per se*, mediate its anti-aggregation and pro-aggregation activities.

Discussion

Originally identified as an acid shock protein, Asr has long been proposed to play a role in the acid tolerance response of enterobacteria.[54] In fact, the expression of Asr is controlled by at least three two-component systems (i.e., PhoQP-RstBA, BasSR, and PhoRB), which sense the levels of Mg^{2+}, Zn^{2+}, and phosphate apart from H^+.[49,54–56] The deletion of *asr* in *E. coli* or its homologous gene in *Salmonella enterica* serovar Typhimurium decreases their capability to infect hosts.[57,58] However, the molecular functions and properties of Asr remain poorly understood. In this study, we showed that Asr is an intrinsically disordered chaperone that affects protein aggregation, and the effect depends on the net charges of its client proteins. The similarity between the net charges of Asr and client proteins drives the anti-aggregation activity of Asr. When carrying the opposite net charges to client proteins, Asr shows the aggregation-promoting activity. Further tests showed that these two distinct activities were considerably affected by the positively charged residues of Asr. Net-charge regulation in chaperone activity may represent an alternative working model of highly charged chaperones.

We proposed a working model based on the net-charge-dependent activity of Asr. In this model, Asr can associate firmly or loosely with its clients depending on their net charges, thereby changing the clients' propensity to aggregate (Figure 5). When a client and Asr have opposite charges, the binding of Asr minimizes the intermolecular repulsion of the client owing to the neutralization of the client's net charges. This allows the exposed hydrophobic patches in non-native protein molecules to interact, which accelerates client aggregation. However, when Asr and the client carry positive net charges, the intermolecular repulsion of the client is strengthened because of Asr binding, which further increases the net charges of the client. This effect impedes collisions among exposed hydrophobic patches, thereby reducing aggregation.

The molecular nature of Asr as a hydrophilic, charged, and disordered polymer is reminiscent of similar molecules that exert protective effects against protein instability and aggregation. As

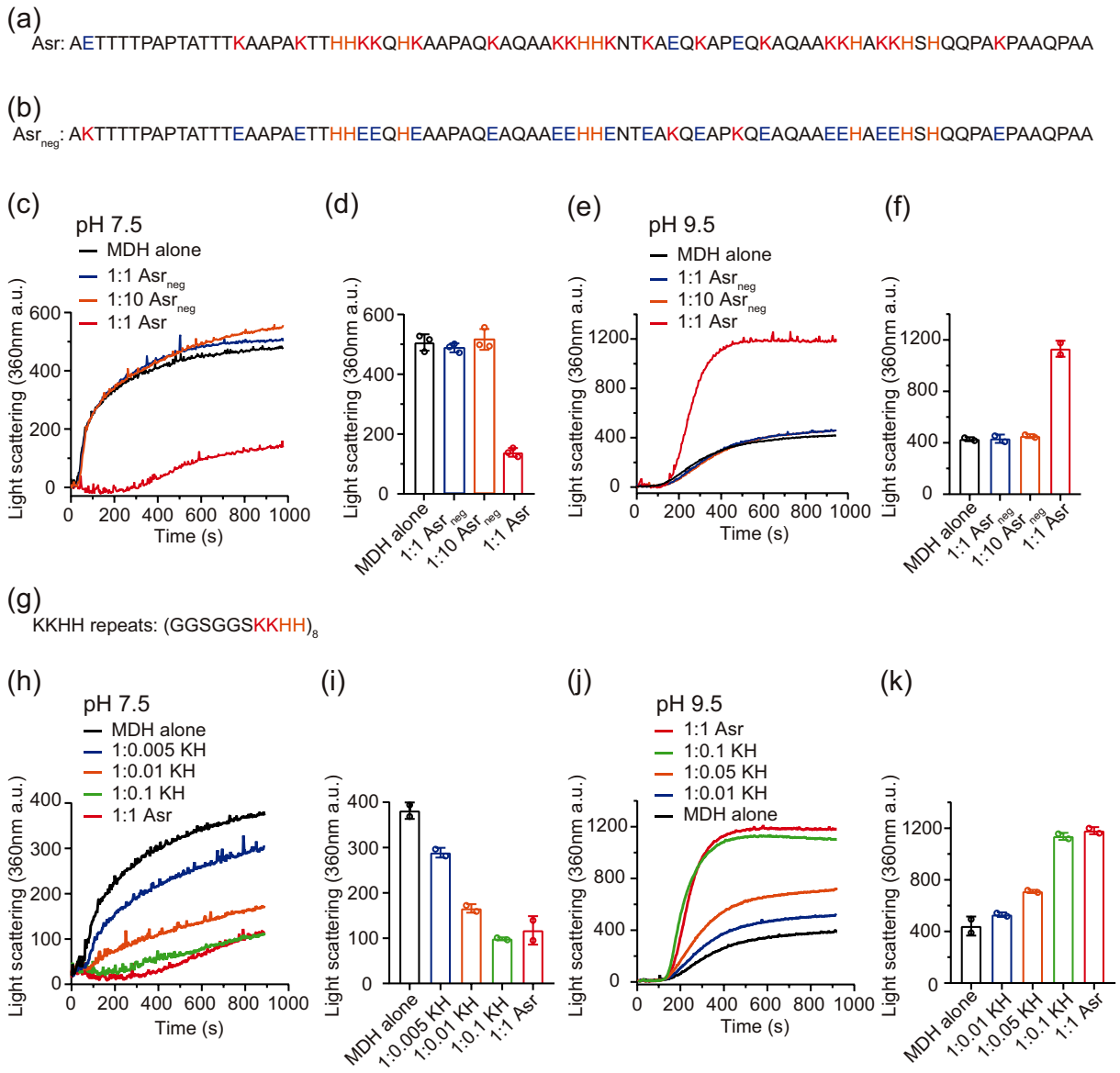

Figure 4. Positively charged residues within Asr mediate its anti-aggregation and pro-aggregation activities. (a and b) Amino acid sequences of Asr (a) and the negatively charged variant, Asr$_{neg}$ (b). Lysine, glutamine acid, and histidine are colored in red, blue, and yellow, respectively. (c and e) Aggregation of thermally denatured MDH alone, in the presence of Asr, or in the presence of increasing amounts of Asr$_{neg}$ at pH 7.5 (c) or pH 9.5 (e). (d and f) Quantification of light-scattering values in panels (c) and (e) at the 15 min time point. (g) The amino acid sequence of the KKHH peptide. (h and j) Aggregation of thermally denatured MDH alone, in the presence of Asr, or the presence of increasing amounts of the KKHH peptide at pH 7.5 (h) or pH 9.5 (j). (i and k) Quantification of light-scattering values in panels (h) and (j) at the 15 min time point. Experiments were conducted at least twice, and representative curves are shown. Data were presented as the mean ± SD.

intrinsically disordered chaperones, late embryogenesis abundant (LEA) proteins are known for their anti-aggregation activities under desiccation or osmotic stresses.[59] Hydrophilic and charged residues in these proteins are proposed to enable the conservation of water around clients during dehydration. It is also assumed that the disordered regions within LEA proteins underline the capability to exert protective effects against protein instability and aggregation because of their structural flexibility and the ability to bind to a wide range of clients.[8] Hero proteins are active and protein-protective components in the boiled supernatants of crude cell lysates. They tend to be structurally disordered and highly charged.[28] In addition to some highly charged proteins, biological molecules, such as polyelectrolytes,[60] nucleic acids,[25,26] polyphosphates,[27] and ATP,[61] are considered

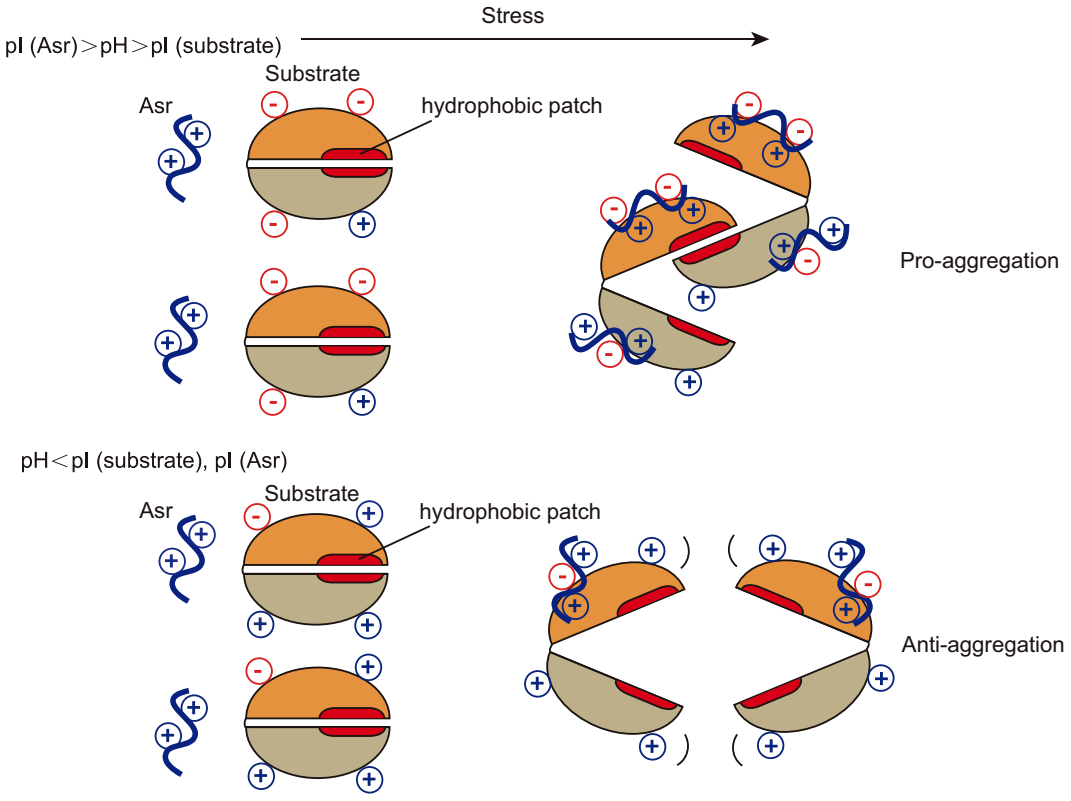

Figure 5. Model for the effects of Asr on protein aggregation. Cellular and physical stresses cause conformational fluctuations in proteins that alter the exposure of their hydrophobic patches, enabling protein molecules to associate through hydrophobic effects and form aggregates. Given that molecules with the same charge tend to repel one another, aggregation occurs when intermolecular electrostatic repulsion is offset. When the client and Asr have opposite net charges (top), the binding of positively charged Asr reduces the overall net charges of the client (originally carrying negative charges), thereby promoting the intermolecular interactions of exposed hydrophobic patches in the client and aggregation. When the client and Asr are both positively charged (bottom), the weak binding of the positively charged Asr to the client's negatively charged local surface further increases the overall net charges of the client, thus enhancing the electrostatic repulsion between client molecules and suppressing aggregation.

chaperones because of their protein-protective effects. Therefore, a bioinformatic search on Asr-like proteins and their characterization is expected to enhance our understanding of these non-canonical chaperone molecules.

Molecular chaperones usually have diverse and sometimes paradoxical activities under different conditions. For instance, the function of the oxidative-activated chaperone Hsp33 is determined by redox conditions. Oxidized Hsp33 functions as a chaperone that inhibits protein aggregation[6,14] and reduced Hsp33 catalyzes the aggregation of elongation factor thermo unstable (EF-Tu).[62] This functional transition is caused by the reduction of the C-terminal redox switch domain, which inactivates the holding activity of the chaperone and evokes its inherent function as an unfoldase. The Hsc70 co-chaperone CHIP (carboxyl terminus of Hsc70-interacting protein) suppresses the aggregation of huntingtin or ataxin-3 but promotes the aggregation of ataxin-1, exerting substrate-specific and context-dependent effects.[63] The contradictory functions of polyphosphates and DNA have been reported. In addition to their aggregation-preventing chaperone activities, they instigate the formation of soluble oligomers with the amyloid-like properties of some client proteins.[64–66] Our work showed that pH could regulate the transition of Asr between functioning as a chaperone and functioning as an aggregase by changing the net charges of client proteins. Conditional regulation of the functions of these chaperones may enable cells to survive under variable environmental conditions and stress.

How does the current working model of Asr implicate its function *in vivo*? When *E. coli* is subjected to mildly acidic stress, such as pH 4.5, the periplasm nearly instantaneously equilibrates with the environmental pH due to the rapid influx of protons. More than 95% of proteins in the periplasm have pI values higher than 4.5 and thus carry positive net charges similar to Asr (Figure S10). Therefore, sharply induced Asr can exert a promiscuous protective effect on these

proteins and thereby facilitate proteostasis in the periplasm.

In addition to acidic stress, other stresses, such as copper, oxidative, and alcohol stress, can induce Asr (Figure 2(b)). Can the net-charge regulated chaperone mechanism of Asr revealed under mildly acidic conditions be extended to other *asr*-inducing conditions? It is worth mentioning that the interplay between different tolerance mechanisms *in E. coli* toward different stressors has been reported due to the cross-activation of different stress-response pathways.[67] For instance, alcohol stress can activate various networks of stress responses, such as envelope stress, oxidative stress, and acidic stress responses in bacteria.[68] Notably, alcohol can disrupt the integrity of the cell membrane and alter the metabolic pathway that accumulates acetate in *E. coli*,[69,70] thereby facilitating the excretion of protons from the cytoplasm into culture media. As the pH of the periplasm decreases, the number of proteins in the periplasm that carry positive net charges similar to Asr increases, and Asr may provide protection to these proteins. Therefore, the chaperone effect of Asr may not be specific to acidic stress and may be of general significance.

Furthermore, it is noteworthy that 15% of all disordered proteins are capable of binding lipids.[71,72] Given our observations that the lipid-like molecule SDS and liposomes interact with Asr, we hypothesized that Asr might bind to bacterial membranes *in vivo* through electrostatic interactions between its positively charged side chains and anionic phospholipids in the bacterial membrane. These interactions may enable Asr to maintain the proteostasis of OMPs, such as OmpC, under external stress. Mature OmpC possesses a theoretical pI value of 4.48. At pH 4.5, the net charge of OmpC is close to zero. Thus, Asr may maintain the proteostasis of OmpC mainly through its protective effects on outer membrane integrity rather than through direct interaction with OmpC. In addition, many IDPs and highly charged molecules (e.g., nucleic acids and polyphosphates) can participate in liquid–liquid phase separation (LLPS).[73–75] As a future perspective, determining whether Asr undergoes LLPS in response to stimuli in cellular physicochemical environments may be of great significance. If this is the case, a thorough characterization of Asr can help discover novel membrane-less compartments in the bacterial periplasm.

In conclusion, we have uncovered the role of Asr in affecting protein aggregation, which revealed net-charge regulation in chaperone activity. Our findings provide a solid foundation for engineering other net charge-dependent chaperones that may be useful for industrial biotechnology and pharmaceuticals. Based on anti-aggregation activity, Asr and its derivative proteins (e.g., KKHH repeats) can act as stabilizers at all stages of development and for the manufacture of biocatalysts and protein therapeutics. Regarding pro-aggregation activity, Asr and its derivative proteins can be deployed to selectively precipitate unwanted proteins from biocatalytic or purification reactions or to suppress the toxicity of neurodegeneration-related oligomers by driving them into insoluble large aggregates or amyloids. We further expect that the mechanistic analysis of the chaperone action of Asr-like molecules will open the door to the *de novo* design of artificial chaperones and the development of future therapeutic agents.

Materials and Methods

Strains, plasmids, and growth conditions

All strains and plasmids used in this work are listed in **Table S2** in the Supplemental Materials. *E. coli* Trans1 T1 (TransGen Biotech), BL21 (DE3), and MC4100 were used for cloning, protein purification, and the acid survival assay, respectively. The *asr* gene deletion strain was generated using the lambda-derived Red recombination system.[76] Unless otherwise indicated, all strains were grown at 37 °C with shaking in LB. For the acidic stress tests, MC4100 or MC4100-derived strains were grown in a low-phosphate-glucose-salt medium (LPM) buffered at different pH values as described previously.[32,77] The following antibiotics were added to the media when necessary: ampicillin (200 μg/mL) or kanamycin (100 μg/mL).

Plasmid construction was performed using the standard restriction enzyme cloning technique or overlap extension PCR cloning technique as described previously.[78] The sequence of the *asr* operon was amplified from the genomic DNA as described previously.[54] Plasmid pRC was generated by replacing the L-arabinose operon in pBAD43 with the operon of the *asr* gene. For protein expression, the corresponding encoding sequences were cloned into a pET28b-based vector containing an N-terminal His-SUMO tag. Genes encoding Asr_{neg} and KH protein were synthesized by Tsingke Biotechnology, and genes encoding the proteins of *E. coli* were directly amplified from the genomic DNA. To detect the absorbance of the proteins without tryptophan and tyrosine during purification at 280 nm, the codon encoding tyrosine was added in front of the stop codon in the encoding sequences of the proteins. All constructs were confirmed through sequencing.

qRT-PCR analysis

E. coli MC4100 wild-type and *asr* deletion strains were grown overnight in LPM buffered at pH 7.0. The overnight culture was then diluted to an

OD_{600} of 0.02 in fresh LPM buffered at pH 7.0 and further grown at 37 °C until an OD_{600} of 0.5 was reached. Cells were then changed to fresh LPM buffered at pH 7.0 or pH 4.5. After incubation at 37 °C for 1 h, the shocked cells with a total OD_{600} of 1 were pelleted by centrifugation at 1000*g* for 2 min.

Next, total RNA was isolated using TRIzol (TransGen Biotech, China) according to the manufacturer's instructions. The purified RNA (1 μg) was used for cDNA synthesis through reverse-transcription polymerase chain reaction according to ReverTra Ace® qPCR RT Master Mix with gDNA Remover (TOYOBO, Japan) instructions. For quantitative PCR, 2 μL of cDNA was mixed with 10 μL of THUNDERBIRD SYBR® qPCR Mix (TOYOBO, Japan) and 8 μL of primer mix (*asr*-F: ACTGCGACGACCACCAAAGC; *asr*-R: GCCTGCGCTTTTTGTTCAGGG; final concentration of each primer was 0.4 μM in the reaction). Reactions were carried out in a CFX96 real-time PCR detection system (Bio-Rad) according to the manufacturer's instructions. The threshold cycle (C_T) of each gene was calculated using CFX Manager (Bio-Rad). Data were normalized to the abundance of *dna*Q amplified with primers *dna*Q-F: ACCGAAACCACCGGTA TGAAC and *dna*Q-R: ACCACTTCAACGGCACC AAT.

Acid survival and SDS/EDTA or novobiocin sensitivity assays

Acid survival assays were performed as described previously with minor modifications.[32] Briefly, *E. coli* MC4100 wild-type and *asr* deletion strains containing the pRC-*asr* or empty vector were grown overnight in LPM buffered at pH 7.0. The cells were then diluted into LPM buffered at pH 4.5 to an OD_{600} of 0.0001. Then, 200 μL of the culture was inoculated into each well of a honeycomb 100-well plate (cat no. 95025BIO). Cell growth was monitored by using a photometric microplate absorbance reader, Bioscreen C MBR. The plate was incubated at 37 °C for 24 h with continuous shaking, and an OD_{600} reading was performed every 30 min.

For the SDS/EDTA and novobiocin sensitivity assay, *E. coli* MC4100 wild-type and *asr* deletion strains were grown overnight in LPM buffered at pH 7.0. The cells were then diluted into LPM buffered at pH 4.5 or pH 7.0 to an OD_{600} of 0.02. After incubation at 37 °C for 8 h with shaking (220 rpm), the cells were collected through centrifugation and resuspended in phosphate-buffered saline (PBS) to an OD_{600} of 0.5. Ten-fold serial dilutions of the culture were spotted onto LB plates or LB plates supplemented with 0.5% SDS + 0.8 mM EDTA or 30 μg/mL novobiocin. Plates were then incubated at 37 °C for 24 h.

Western blotting

E. coli MC4100 wild-type and *asr* deletion strains were grown overnight in LPM buffered at pH 7.0. Overnight cultures were diluted into fresh LPM medium buffered at pH 4.5 to an OD_{600} of 0.02. After incubation at 37 °C for 9 h with shaking, the cells were pelleted through centrifugation and resuspended in LPM buffered at pH 4.5 to an OD_{600} of 0.5. Approximately 1 mL of each culture was pelleted and resuspended in 1 × urea-SDS sample buffer (60 mM Tris-HCl, pH 6.8, 2% SDS, 4 M urea, 5 mM EDTA, 5% glycerol, 0.005% bromophenol blue, and 1% β-ME).[79] Samples were boiled for 10 min and centrifuged for 1 min (20,000*g*) to eliminate insoluble material before loading to SDS-PAGE.

For immunoblotting, the proteins were transferred from protein gels to polyvinylidene fluoride membranes (Merck) using wet transfer apparatus (Bio-Rad). Membranes were blocked with 5% non-fat milk in TBST (Tris buffer saline containing 0.1% Tween-20) for 1 h at room temperature and then incubated with primary antibody at 4 °C overnight. A 1:1000 dilution of anti-OmpC antibody (cat no. orb6940, Biorbyt), a 1:800 dilution of anti-OmpA antibody, and a 1:2000 dilution of anti-trigger factor (cat no. A01388-40, GenScript) were used. The anti-OmpA antibody was prepared by HangZhou HuaAn Biotechnology Co., Ltd, and purified $OmpA_{203\text{-}346}$ was used as the antigen. After washing with TBST buffer at least three times, the membranes were incubated with IRDye 800 CW secondary antibodies (cat no. 926–32211, LI-COR Biosciences) at a 1:10,000 dilution. After incubation at room temperature for 1 h, the membranes were washed with TBST at least three times and visualized using Odyssey Sa (LI-COR Biosciences). For quantification, the amount of target protein was normalized to the amount of anti-trigger factor.

Protein expression and purification

For protein expression, *E. coli* BL21 (DE3) cells harboring pET28b-based vectors fused with different target proteins were grown at 37 °C overnight with shaking. The overnight culture was diluted into 1 L of LB medium supplemented with 100 μg/mL kanamycin and grown at 37 °C with shaking until an OD_{600} of 0.6 was reached. The expression of target proteins was induced by the addition of isopropyl-β-D-thiogalactoside to a final concentration of 0.1 mM. The culture was grown further at 22 °C with shaking for 16 h.

After centrifugation at 4 °C for 30 min, the cell pellet was resuspended in chilled lysis buffer (50 mM Tris, 400 mM NaCl, 10% glycerol, pH 8.0) with 0.1 mg/mL lysozyme and 1 × protein inhibitor cocktail (Sigma). The cells were then lysed using a high-pressure cell disruptor for 10 min at 800 psi. The lysate was cleared through centrifugation

for 1 h at 10,000*g* at 4 °C, and the supernatant was incubated with 2 mL of cOmplete™ His-Tag purification resin (Roche) at 4 °C for 2 h with gentle rotation. The resin was washed with chilled lysis buffer, and the target protein was then eluted in lysis buffer supplemented with 300 mM imidazole. The protein solution was dialyzed overnight into buffer A in the presence of ULP1 for cleavage of the His-SUMO tag. Target proteins were loaded onto 5 mL HiTrap SP/Q FF columns equilibrated in buffer A at 4 °C and eluted over a gradient of 0–80% buffer B. Fractions containing target protein were pooled, concentrated, and flash-frozen in liquid nitrogen before they were stored at − 80 °C. Prior to each experiment, target proteins were exchanged into the indicated assay buffer with desalting columns. For purification of Asr, YhhA, and KKHH repeats, the HiTrap SP FF column was used with buffer A (20 mM HEPES, 0.5 mM EDTA, pH 7.0) and buffer B (20 mM HEPES, 0.5 mM EDTA, 1 M NaCl, pH 7.0). For the purification of YjdP, YbgS, and Asr_{neg}, a HiTrap Q FF column was used with buffer A (20 mM sodium acetate, 0.5 mM EDTA, pH 5.6) and buffer B (20 mM sodium acetate, 0.5 mM EDTA, 1 M NaCl, pH 5.6).

Circular dichroism

All CD spectra were obtained using a Chirascan circular dichroism spectrometer (Applied Photophysics Ltd) at 20 °C unless otherwise specified. The CD measurements were taken from 260 nm to 180 nm at 1 nm intervals and a 1 nm/s scanning rate. For the CD spectra of Asr, 10 μM protein in 10 mM potassium phosphate buffered at different pH values or supplemented with urea and SDS was placed in a 1 mm quartz cuvette. Temperature-dependent CD spectra were captured at 10 °C intervals from 10 °C to 80 °C at a ramp rate of 1 °C/min. For CD spectra of KKHH repeats and Asr_{neg}, 10 μM protein in 10 mM potassium phosphate buffered at the indicated pH values was placed in a 1 mm quartz cuvette. For the CD spectra of client proteins, the indicated concentrations of protein in 10 mM potassium phosphate buffered at the indicated pH values were placed in a 1 mm quartz cuvette.

Aggregation assays

Malate dehydrogenase (MDH) from pig heart mitochondria was purchased from Roche (10127256001). Citrate synthase (CS) from pig hearts was purchased from Sigma (C3260). MDH and CS were dialyzed extensively into 50 mM potassium phosphate and 0.5 mM EDTA at pH 7.5 to completely remove ammonium sulfate and stored at −80 °C until use. QuantiLum recombinant luciferase (Luc) from the North American firefly was purchased from Promega (cat no. E1702) and stored at −80 °C until use.

For chemically induced aggregation, 50 μM MDH was denatured in 6.6 M urea with 10 mM DTT for 2 h at room temperature and then diluted to a final concentration of 0.5 μM in 40 mM HEPES-KOH at pH 7.5 with constant stirring at 30 °C in the absence or presence of various concentrations of Asr. For thermally induced aggregation, MDH was diluted to a final concentration of 0.5 μM in assay buffers containing 10 mM potassium phosphate, pH 4.5; 40 mM HEPES-KOH, pH 7.5; or 40 mM glycine-NaOH, pH 9.5 with constant stirring at 43 °C in the absence or presence of various concentrations of test molecules. Luc was diluted to a final concentration of 0.13 μM in 10 mM potassium phosphate buffered at the indicated pH values with constant stirring at 43 °C in the absence or presence of various concentrations of test molecules. CS was diluted to a final concentration of 0.15 μM in 10 mM potassium phosphate buffered at the indicated pH values with constant stirring at 43 °C in the absence or presence of various concentrations of test molecules. Light scattering was measured at 360 nm with a Thermo LUMINA fluorescence spectrophotometer equipped with temperature-controlled sample holders.

Computational analysis

All 327 periplasmic (according to STEPdb annotation) protein sequences were retrieved from UniProt. All signal peptide sequences were removed according to PTM/processing sections in UniProt by a Python script. The pI value and hydrophobic score (GRAVY) of all processed sequences were calculated using the ProtParam module in the BioPython package. The disorder content of each sequence was retrieved using the MobiDB official API. A total of 20 canonical amino acids were included in the amino acid composition calculation. Selenocysteine (U) and unknown amino acids (X) were omitted for simplicity. The count of selenocysteine (U) was 3, whereas that of the unknown amino acid (X) was 8 in the *E. coli* proteome (UP000000625). Neither affected the overall amino acid composition calculation. The amino acid composition of Asr with its signal peptide removed and the *E. coli* proteome (UP000000625) was calculated using a Python script. The categorized amino acid composition data were then mapped to a radar map with the Matplotlib and NumPy packages. Anaconda distribution of Python 3.7.3 with Spyder integrated development environment was used in making Python scripts. All programs were processed on Intel Core i5-10400F.

Data Availability

All data used in this study are included in this published article (and its supplementary

information files) and are available from the corresponding author upon reasonable request.

CRediT authorship contribution statement

Chang Ren: Conceptualization, Methodology, Investigation, Data curation, Writing – original draft, Writing – review & editing. **Yongxin Zheng:** Investigation, Resources, Data curation, Validation, Formal analysis. **Chunlan Liu:** Visualization, Investigation. **Jun Mencius:** Software, Writing – review & editing. **Zhili Wu:** Resources, Validation. **Shu Quan:** Conceptualization, Supervision, Writing – review & editing, Funding acquisition, Project administration.

Acknowledgments

We thank Cuiting Yang for the assistance in the initial stages of this study. We acknowledge all members of our laboratory for their technical support and helpful recommendations.

This work was supported by National Natural Science Foundation of China (NSFC) grants 32171269 and 31661143021(to S.Q.), the Fundamental Research Funds for the Central Universities (22221818014 to S.Q.), the Research Program of State Key Laboratory of Bioreactor Engineering (to S.Q.), and a grant from Shanghai Frontiers Science Center of Optogenetic Techniques for Cell Metabolism (Shanghai Municipal Education Commission, grant 2021 Sci & Tech 03-28).

Declaration of Competing Interest

The authors declare that they have no competing interests.

Author contributions

C.R. and S.Q. conceived the study. C.R., Y.Z., C. L., J.M, and Z.W. performed the experiments and analyzed the data. C.R., J.M., and S.Q. wrote the manuscript.

Appendix A. Supplementary data

Supplementary data to this article can be found online at https://doi.org/10.1016/j.jmb.2021.167405.

Received 13 August 2021;
Accepted 8 December 2021;
Available online 13 December 2021

Keywords:
chaperone;
intrinsically disordered protein;
net-charge regulation;
protein aggregation;
stress response

† C.R. and Y.Z. contributed equally to this work.

Abbreviations used:
Hero, heat-resistant obscure; IDP, intrinsically disordered protein; CD, circular dichroism; PPII, polyproline II; SDS, sulfate dodecyl sodium; EDTA, ethylene diamine tetraacetic acid; LPM, low-phosphate-glucose-salt medium; OmpA, outer membrane protein A; OmpC, outer membrane porin C; MDH, malate dehydrogenase; Luc, luciferase; CS, citrate synthase; pI, isoelectric point; LEA, late embryogenesis abundant; ATP, adenosine triphosphate; EF-Tu, elongation factor thermal-unstable; CHIP, carboxyl terminus of Hsc70-interacting protein; LLPS, liquid–liquid phase separation

References

1. Goto, Y., Fink, A.L., (1994). Acid-induced folding of heme proteins. *Methods Enzymol.* **232**, 3–15.
2. Weijers, M., Barneveld, P.A., Stuart, M.A.C., Visschers, R. W., (2003). Heat-induced denaturation and aggregation of ovalbumin at neutral pH described by irreversible first-order kinetics. *Protein Sci.* **12**, 2693–2703.
3. Aseervatham, G.S., Sivasudha, T., Jeyadevi, R., Arul Ananth, D., (2013). Environmental factors and unhealthy lifestyle influence oxidative stress in humans–an overview. *Environ. Sci. Pollut. Res. Int.* **20**, 4356–4369.
4. Franzmann, T.M., Menhorn, P., Walter, S., Buchner, J., (2008). Activation of the chaperone Hsp26 is controlled by the rearrangement of its thermosensor domain. *Mol. Cell* **29**, 207–216.
5. Voth, W., Schick, M., Gates, S., Li, S., Vilardi, F., Gostimskaya, I., et al., (2014). The protein targeting factor Get3 functions as ATP-Independent chaperone under oxidative stress conditions. *Mol. Cell* **56**, 116–127.
6. Winter, J., Ilbert, M., Graf, P.C.F., Özcelik, D., Jakob, U., (2008). Bleach activates a redox-regulated chaperone by oxidative protein unfolding. *Cell* **135**, 691–701.
7. Hong, W., Jiao, W., Hu, J., Zhang, J., Liu, C., Fu, X., et al., (2005). Periplasmic protein HdeA exhibits chaperone-like activity exclusively within stomach pH range by transforming into disordered conformation. *J. Biol. Chem.* **280**, 27029–27034.
8. Suss, O., Reichmann, D., (2015). Protein plasticity underlines activation and function of ATP-independent chaperones. *Front. Mol. Biosci.* **2**, 43.
9. Bardwell, J.C., Jakob, U., (2012). Conditional disorder in chaperone action. *Trends Biochem. Sci.* **37**, 517–525.
10. Kim, H., Wu, K., Lee, C., (2021). Stress-responsive periplasmic chaperones in bacteria. *Front. Mol. Biosci.* **8**, 678697
11. Saibil, H., (2013). Chaperone machines for protein folding, unfolding and disaggregation. *Nature Rev. Mol. Cell Biol.* **14**, 630–642.
12. Tompa, P., Csermely, P., (2004). The role of structural disorder in the function of RNA and protein chaperones. *FASEB J.* **18**, 1169–1175.

13. Reichmann, D., Jakob, U., (2013). The roles of conditional disorder in redox proteins. *Curr. Opin. Struct. Biol.* **23**, 436–442.
14. Reichmann, D., Xu, Y., Cremers, C.M., Ilbert, M., Mittelman, R., Fitzgerald, M.C., et al., (2012). Order out of disorder: working cycle of an intrinsically unfolded chaperone. *Cell* **148**, 947–957.
15. Yu, X.C., Hu, Y., Ding, J., Li, H., Jin, C., (2019). Structural basis and mechanism of the unfolding-induced activation of HdeA, a bacterial acid response chaperone. *J. Biol. Chem.* **294**, 3192–3206.
16. Koldewey, P., Stull, F., Horowitz, S., Martin, R., Bardwell, J.C., (2016). Forces driving chaperone action. *Cell* **166**, 369–379.
17. Kim, Y.E., Hipp, M.S., Bracher, A., Hayer-Hartl, M., Hartl, F.U., (2013). Molecular chaperone functions in protein folding and proteostasis. *Annu. Rev. Biochem.* **82**, 323–355.
18. Saio, T., Guan, X., Rossi, P., Economou, A., Kalodimos, C. G., (2014). Structural basis for protein antiaggregation activity of the trigger factor chaperone. *Science* **344**
19. Liu, W., Bratko, D., Prausnitz, J.M., Blanch, H.W., (2003). Electrostatic interactions between peptides and the molecular chaperone DnaK. *J. Phys. Chem. B* **107**, 11563–11569.
20. Koldewey, P., Horowitz, S., Bardwell, J.C.A., (2017). Chaperone-client interactions: non-specificity engenders multifunctionality. *J. Biol. Chem.* **292**, 12010–12017.
21. Schreiber, G., Haran, G., Zhou, H.X., (2009). Fundamental aspects of protein - protein association kinetics. *Chem. Rev.* **109**, 839–860.
22. Perrett, S., Zahn, R., Stenberg, G., Fersht, A.R., (1997). Importance of electrostatic interactions in the rapid binding of polypeptides to GroEL. *J. Mol. Biol.* **269**, 892–901.
23. Hagn, F., Lagleder, S., Retzlaff, M., Rohrberg, J., Demmer, O., Richter, K., et al., (2010). Structural analysis of the interaction between Hsp90 and the tumor suppressor protein p53. *Nature Struct. Mol. Biol.* **18**, 1086–1093.
24. He, W., Zhang, J., Sachsenhauser, V., Wang, L., Bardwell, J.C.A., Quan, S., (2020). Increased surface charge in the protein chaperone Spy enhances its anti-aggregation activity. *J. Biol. Chem.* **295**, 14488–14500.
25. Docter, B.E., Horowitz, S., Gray, M.J., Jakob, U., Bardwell, J.C., (2016). Do nucleic acids moonlight as molecular chaperones? *Nucleic Acids Res.* **44**, 4835–4845.
26. Begeman, A., Litberg, T.J., Bourne, J., Xuan, Z., Horowitz, S., (2020). G-Quadruplexes act as sequence-dependent protein chaperones. *EMBO Rep.* **21**, e49735
27. Gray, M.J., Wholey, W.Y., Wagner, N.O., Cremers, C.M., Mueller-Schickert, A., Hock, N.T., et al., (2014). Polyphosphate is a primordial chaperone. *Mol. Cell* **53**, 689–699.
28. Tsuboyama, K., Osaki, T., Matsuura-Suzuki, E., Kozuka-Hata, H., Okada, Y., Oyama, M., et al., (2020). A widespread family of heat-resistant obscure (Hero) proteins protect against protein instability and aggregation. *PLoS Biol.* **18**, e3000632
29. Koebnik, R., Locher, K.P., Van Gelder, P., (2000). Structure and function of bacterial outer membrane proteins: Barrels in a nutshell. *Mol. Microbiol.* **37**, 239–253.
30. Quan, S., Koldewey, P., Tapley, T., Kirsch, N., Ruane, K. M., Pfizenmaier, J., et al., (2011). Genetic selection designed to stabilize proteins uncovers a chaperone called Spy. *Nature Struct. Mol. Biol.* **18**, 262–269.
31. Seputiene, V., Suziedelis, K., Normark, S., Melefors, O., Suziedeliene, E., (2004). Transcriptional analysis of the acid-inducible asr gene in enterobacteria. *Res. Microbiol.* **155**, 535–542.
32. Šeputiene, V., Motiejunas, D., Sužiedelis, K., Tomenius, H., Normark, S., Melefors, Ö., et al., (2003). Molecular characterization of the acid-inducible asr gene of Escherichia coli and its role in acid stress response. *J. Bacteriol.* **185**, 2475–2484.
33. Eilers, M., Shekar, S.C., Shieh, T., Smith, S.O., Fleming, P. J., (2000). Internal packing of helical membrane proteins. *Proc. Natl. Acad. Sci. USA* **97**, 5796–5801.
34. Pinker, R.J., Lin, L., Kallenbach, N.R., Rose, G.D., (1993). Effects of alanine substitutions in α-helices of sperm whale myoglobin on protein stability. *Protein Sci.* **2**, 1099–1105.
35. Kyte, J., Doolittle, R.F., (1982). A simple method for displaying the hydropathic character of a protein. *J. Mol. Biol.* **157**, 105–132.
36. Dosztányi, Z., Csizmok, V., Tompa, P., Simon, I., (2005). IUPred: Web server for the prediction of intrinsically unstructured regions of proteins based on estimated energy content. *Bioinformatics* **21**, 3433–3434.
37. Tran, H.T., Wang, X., Pappu, R.V., (2005). Reconciling observations of sequence-specific conformational propensities with the generic polymeric behavior of denatured proteins. *Biochemistry* **44**, 11369–11380.
38. Fitzkee, N.C., Rose, G.D., (2004). Reassessing random-coil statistics in unfolded proteins. *Proc. Natl. Acad. Sci. USA* **101**, 12497–12502.
39. Zagrovic, B., Lipfert, J., Sorin, E.J., Millett, I.S., Van Gunsteren, W.F., Doniach, S., et al., (2005). Unusual compactness of a polyproline type II structure. *Proc. Natl. Acad. Sci. USA* **102**, 11698–11703.
40. Zhu, F., Kapitan, J., Tranter, G.E., Pudney, P.D.A., Isaacs, N.W., Hecht, L., et al., (2008). Residual structure in disordered peptides and unfolded proteins from multivariate analysis and ab initio simulation of Raman optical activity data. *Proteins* **70**, 823–833.
41. Elam, W.A., Schrank, T.P., Campagnolo, A.J., Hilser, V.J., (2013). Evolutionary conservation of the polyproline II conformation surrounding intrinsically disordered phosphorylation sites. *Protein Sci.* **22**, 405–417.
42. Tiffany, M.L., Krimm, S., (1973). Extended conformations of polypeptides and proteins in urea and guanidine hydrochloride. *Biopolymers* **12**, 575–587.
43. Chin, A.F., Toptygin, D., Elam, W.A., Schrank, T.P., Hilser, V.J., (2016). Phosphorylation Increases Persistence Length and End-to-End Distance of a Segment of Tau Protein. *Biophys. J.* **110**, 362–371.
44. Chemes, L.B., Alonso, L.G., Noval, M.G., De Prat-Gay, G., (2012). Circular dichroism techniques for the analysis of intrinsically disordered proteins and domains. *Methods Mol. Biol.* **895**, 387–404.
45. Jephthah, S., Staby, L., Kragelund, B.B., Skepö, M., (2019). Temperature dependence of intrinsically disordered proteins in simulations: what are we missing? *J. Chem. Theory Comput.* **15**, 2672–2683.
46. Kjaergaard, M., Nørholm, A.B., Hendus-Altenburger, R., Pedersen, S.F., Poulsen, F.M., Kragelund, B.B., (2010). Temperature-dependent structural changes in intrinsically disordered proteins: Formation of α-helices or loss of polyproline II? *Protein Sci.* **19**, 1555–1564.
47. Sun, Y., Zhang, J., Wang, H., Wang, T., Cheng, H., Yu, B., et al., (2018). Sulfate dodecyl sodium-induced stability of a

model intrinsically disordered protein, bovine casein. *Food Hydrocoll.* **82**, 19–28.
48. Hong, Z., Damodaran, K., Asher, S.A., (2014). Sodium dodecyl sulfate monomers induce XAO peptide polyproline II to α-helix transition. *J. Phys. Chem. B* **118**, 10565–10575.
49. Tucker, D.L., Tucker, N., Conway, T., (2002). Gene expression profiling of the pH response in Escherichia coli. *J. Bacteriol.* **184**, 6551–6558.
50. Hishiya, A., Takayama, S., (2008). Molecular chaperones as regulators of cell death. *Oncogene* **27**, 6489–6506.
51. Falchi, F.A., Maccagni, E.A., Puccio, S., Peano, C., De Castro, C., Palmigiano, A., et al., (2018). Mutation and suppressor analysis of the essential lipopolysaccharide transport protein LptA reveals strategies to overcome severe outer membrane permeability defects in Escherichia coli. *J. Bacteriol.* **200**, e00487–e517.
52. Nikaido, H., (2003). Molecular basis of bacterial outer membrane permeability revisited. *Microbiol. Mol. Biol. Rev.* **67**, 593–656.
53. Choi, U., Lee, C.R., (2019). Distinct roles of outer membrane porins in antibiotic resistance and membrane integrity in Escherichia coli. *Front. Microbiol.* **10**, 953.
54. Sužiedeliene, E., Sužiedelis, K., Garbenčiute, V., Normark, S., (1999). The acid-inducible asr gene in Escherichia coli: Transcriptional control by the phoBR operon. *J. Bacteriol.* **181**, 2084–2093.
55. Ogasawara, H., Hasegawa, A., Kanda, E., Miki, T., Yamamoto, K., Ishihama, A., (2007). Genomic SELEX search for target promoters under the control of the PhoQP-RstBA signal relay cascade. *J. Bacteriol.* **189**, 4791–4799.
56. Lee, L.J., Barrett, J.A., Poole, R.K., (2005). Genome-wide transcriptional response of chemostat-cultured Escherichia coli to zinc. *J. Bacteriol.* **187**, 1124–1134.
57. Allam, U.S., Gopala Krishna, M., Sen, M., Thomas, R., Lahiri, A., Gnanadhas, D.P., et al., (2012). Acidic pH induced STM1485 gene is essential for intracellular replication of Salmonella. *Virulence* **3**, 122–135.
58. Armalyte, J., Šeputiene, V., Melefors, O., Sužiedeliene, E., (2008). An Escherichia coli asr mutant has decreased fitness during colonization in a mouse model. *Res. Microbiol.* **159**, 486–493.
59. Kovacs, D., Kalmar, E., Torok, Z., Tompa, P., (2008). Chaperone activity of ERD10 and ERD14, two disordered stress-related plant proteins. *Plant Physiol.* **147**, 381–390.
60. Sofronova, A.A., Izumrudov, V.A., Muronetz, V.I., Semenyuk, P.I., (2017). Similarly charged polyelectrolyte can be the most efficient suppressor of the protein aggregation. *Polymer* **108**, 281–287.
61. Patel, A., Malinovska, L., Saha, S., Wang, J., Alberti, S., Krishnan, Y., et al., (2017). ATP as a biological hydrotrope. *Science* **356**, 753–756.
62. Jo, K.S., Kim, J.H., Ryu, K.S., Kang, J.S., Wang, C.Y., Lee, Y.S., et al., (2019). Unique Unfoldase/Aggregase Activity of a Molecular Chaperone Hsp33 in its Holding-Inactive State. *J. Mol. Biol.* **431**, 1468–1480.
63. Choi, J.Y., Ryu, J.H., Kim, H.S., Park, S.G., Bae, K.H., Kang, S., et al., (2007). Co-chaperone CHIP promotes aggregation of ataxin-1. *Mol. Cell. Neurosci.* **34**, 69–79.
64. Yoo, N.G., Dogra, S., Meinen, B.A., Tse, E., Haefliger, J., Southworth, D.R., et al., (2018). Polyphosphate stabilizes protein unfolding intermediates as soluble amyloid-like oligomers. *J. Mol. Biol.* **430**, 4195–4208.
65. Litberg, T.J., Docter, B., Hughes, M.P., Bourne, J., Horowitz, S., (2020). DNA facilitates oligomerization and prevents aggregation via DNA networks. *Biophys. J.* **118**, 162–171.
66. Zhang, C.M., Yamaguchi, K., So, M., Sasahara, K., Ito, T., Yamamoto, S., et al., (2019). Possible mechanisms of polyphosphate-induced amyloid fibril formation of beta2-microglobulin. *Proc. Natl. Acad. Sci. USA* **116**, 12833–12838.
67. Bury-Moné, S., Nomane, Y., Reymond, N., Barbet, R., Jacquet, E., Imbeaud, S., et al., (2009). Global analysis of extracytoplasmic stress signaling in Escherichia coli. *PLoS Genet.* **5**, e1000651
68. Horinouchi, T., Maeda, T., Furusawa, C., (2018). Understanding and engineering alcohol-tolerant bacteria using OMICS technology. *World J. Microbiol. Biotechnol.* **34**, 157.
69. Cao, H., Wei, D., Yang, Y., Shang, Y., Li, G., Zhou, Y., et al., (2017). Systems-level understanding of ethanol-induced stresses and adaptation in E. coli. *Sci. Rep.* **7**, 44150.
70. Vulić, M., Kolter, R., (2002). Alcohol-induced delay of viability loss in stationary-phase cultures of Escherichia coli. *J. Bacteriol.* **184**, 2898–2905.
71. Fuglebakk, E., Reuter, N., (2018). A model for hydrophobic protrusions on peripheral membrane proteins. *PLoS Comput. Biol.* **14**
72. Deryusheva, E., Nemashkalova, E., Galloux, M., Richard, C.A., Eléouët, J.F., Kovacs, D., et al., (2019). Does intrinsic disorder in proteins favor their interaction with lipids? *Proteomics* **19**, e1800098
73. Posey, A.E., Holehouse, A.S., Pappu, R.V., (2018). Phase separation of intrinsically disordered proteins. *Methods Enzymol.* **611**, 1–30.
74. Wang, X., Shi, C., Mo, J., Xu, Y., Wei, W., Zhao, J., (2020). An inorganic biopolymer polyphosphate controls positively charged protein phase transitions. *Angew. Chem. Int. Ed. Engl.* **59**, 2679–2683.
75. Du, M., Chen, Z.J., (2018). DNA-induced liquid phase condensation of cGAS activates innate immune signaling. *Science* **361**, 704–709.
76. Datsenko, K.A., Wanner, B.L., (2000). One-step inactivation of chromosomal genes in Escherichia coli K-12 using PCR products. *Proc. Natl. Acad. Sci. USA* **97**, 6640–6645.
77. Bailey, S.C., Apirion, D., (1977). Identification of lipopolysaccharides and phospholipids of Escherichia coli in polyacrylamide gels. *J. Bacteriol.* **131**, 347–355.
78. Bryksin, A., Matsumura, I., (2010). Overlap extension PCR cloning: a simple and reliable way to create recombinant plasmids. *Biotechniques* **48**, 463–465.
79. Palomino, C., Marín, E., Fernández, L.Á., (2011). The fimbrial usher FimD follows the surA-BamB pathway for its assembly in the outer membrane of Escherichia coli. *J. Bacteriol.* **193**, 5222–5230.